inter.noise
HAMBURG 2016

# Acoustic particle velocity investigations in aeroacoustics synchronizing PIV and microphone measurements

Lars SIEGEL[1]; Klaus EHRENFRIED[1]; Arne HENNING[1]; Gerrit LAUENROTH[1]; Claus WAGNER[1, 2]

[1] German Aerospace Center (DLR), Institute of Aerodynamics and Flow Technology (AS), Göttingen, Germany

[2] Technical University Ilmenau, Institute of Thermodynamics and Fluid Mechanics, Ilmenau, Germany

## ABSTRACT

The aim of the present study is the detection and visualization of the sound propagation process from a strong tonal sound source in flows. To achieve this, velocity measurements were conducted using particle image velocimetry (PIV) in a wind tunnel experiment under anechoic conditions. Simultaneously, the acoustic pressure fluctuations were recorded by microphones in the acoustic far field. The PIV fields of view were shifted stepwise from the source region to the vicinity of the microphones. In order to be able to trace the acoustic propagation, the cross-correlation function between the velocity and the pressure fluctuations yields a proxy variable for the acoustic particle velocity acting as a filter for the velocity fluctuations. The temporal evolution of this quantity indicates the propagation of the acoustic perturbations. The acoustic radiation of a square rod in a wind tunnel flow is investigated as a test case. It can be shown that acoustic waves propagate from emanating coherent flow structures in the near field through the shear layer of the open jet to the far field. To validate this approach, a comparison with a 2D simulation and a 2D analytical solution of a dipole is performed.

## 1. INTRODUCTION

The localization of noise sources in turbulent flows and the traceability of the acoustic perturbations emanating from the source regions into the far field are still challenging. A methodology to detect the noise sources was recently proposed by (1) which is based on an acoustic analogy as well as on a generalized intensity which is suitable for flow studies. It could be shown that noise sources can be identified by means of synchronized velocity measurements via PIV in the source region and pressure measurements with microphones in the acoustic far field. There, the cross-correlation function of these two quantities served as acoustic variable for the generalized intensity. The divergence of this time-averaged intensity reflected a region with high energy production rates of the acoustic variable in the vicinity downstream of a square rod indicating the area where the acoustic perturbations originate. Though, due to the non-anechoic conditions and the dominating wind tunnel noise in this experiment, it was impossible to detect and visualize the acoustic propagation. Previous works (2,3) concentrated on investigating the aeroacoustic noise generation using simultaneous particle image velocimetry and microphone measurements in the immediate vicinity of the noise source or in the wake of the examined bodies. Further studies (4,5) used time-resolved high speed PIV technique to detect noise sources and to reconstruct the involved pressure fluctuations produced by the flows around different objects.

The present work focusses on the acoustic propagation represented by the acoustic particle velocity. To achieve a proxy variable for the acoustic particle velocity, velocity measurements were conducted synchronously with pressure recordings under anechoic conditions. The velocity fluctuations around a square rod were gained with a two-dimensional, two-component (2D2C) PIV system for fields of view being shifted stepwise from the source region to the acoustic far field. For this experiment, the separation time of the PIV system was adjusted to resolve the acoustic perturbations in the fields of view outside the turbulent flow region. The measurement of the pressure fluctuations were conducted with microphones in the far field. The cross-correlation function of the recorded pressure and velocity

[1,2] lars.siegel@dlr.de; klaus.ehrenfried@dlr.de; arne.henning@dlr.de; gerrit.lauenroth@dlr.de; claus.wagner@dlr.de

fluctuations can be interpreted as a proxy variable for the acoustic particle velocity. Due to the high time resolution of the microphone measurements, the temporal development of this quantity could be traced whereas the PIV measurements deliver the spatial resolution.

The results of the cross-correlation function are compared with a 2D simulation and a 2D analytical solution of a dipole with regard to the acoustic particle velocity to demonstrate that the cross-correlation function can be used to represent to propagation of the acoustic particle velocity. In the case of the 2D simulation, the dipole moves with the same speed as the wind tunnel velocity. From a physical point of view, this is comparable with the noise radiation produced by the flow around a rod. The approach used to determine the cross-correlation function and the scaling procedure which is needed to compare the results of the cross-correlation to the other approaches is presented in the following section 2.1. The chosen simulation parameters and the numerical method used to solve the problem are presented in section 2.2. The 2D analytical solution of the acoustic particle velocity produced by a dipole is based on the convective wave equation in a uniform flow. The mathematical background as well as the used input parameters are described in section 2.3. The experimental setup and the applied technical parameters are presented in chapter 3 followed by the discussion of the results in chapter 4 and a final conclusion.

## 2. THEORETICAL BACKGROUND

### 2.1 Calculation of the cross-correlation function and scaling

The sample cross-correlation function $S_{p,\psi}(\boldsymbol{x},\tau)$ will be defined as

$$S_{p,\psi}(\boldsymbol{x},\tau) = \frac{1}{N}\sum_{i=1}^{N} \psi'(\boldsymbol{x},t_i)\cdot p'(t_i+\tau), \tag{1}$$

where $\psi'(\boldsymbol{x},t_i)$ represents the zero-mean part of a near-field quantity $\psi$ measured at position $\boldsymbol{x}$ and time $t_i$ by the PIV system. In this study, the focus lies on the velocity fluctuations in the direction towards the microphones which means that $\psi' = v'$. The variable $\tau$ is the time shift between the pressure signal $p'$ recorded by the microphones and $\psi'$. The quantity $N$ denotes the overall samples of the PIV measurements which should be large enough ($N = 15000$ in the present case) to achieve statistical convergence. The cross-correlation function can be regarded as a result from a filtering process for the near-field fluctuations, extracting the parts showing a linear dependency with the far field pressure fluctuations. Thus, the velocity fluctuations filtered in this way can be used as a proxy variable for the acoustic particle velocity.

For the sake of comparability with the 2D simulation and the 2D analytical solution respectively, the cross-correlation function was scaled in accordance to the decibel scale

$$L_S = \underbrace{sgn\left(S_{p,\psi}\right)\cdot log\left(\frac{\left|S_{p,\psi}\right|}{c_0\cdot p_0}\right)}_{L_S^*} /max(|L_S^*|). \tag{2}$$

Here $c_0$ is the speed of sound and $p_0$ represents the reference sound pressure ($p_0 = 20$ µPa). Applying the absolute value on the cross-correlation function is necessary as $S_{p,\psi}$ oscillates between positive and negative values. Therefore, the direction of the velocity is maintained in the sign function. The normalization with the global maximum value ensures a uniform scale between 1 and -1 thus improving comparability.

### 2.2 2D simulation of a moving dipole

The 2D simulation of the acoustic particle velocity propagation produced by a moving dipole was carried out with the open source *MATLAB* toolbox *k-Wave*. The toolbox provides the methods needed to compute propagating acoustic waves in 1D, 2D and 3D by solving three coupled first-order partial differential equations (*Euler* equation, mass conservation and pressure-density relation). A k-space pseudo-spectral method is applied for solving the equations using a *Fourier* collocation scheme to calculate the spatial gradients. The temporal gradients are computed with a k-space corrected finite-difference scheme. The solution of the equations as well as the used methods are described in detail in (6 – 8). Furthermore, the toolbox is equipped with a so-called perfectly matched layer (PML) which ensures anechoic conditions at the boundaries of the computational domain.

Basically, the toolbox is designed for acoustic propagation simulations without flow. Thus, to simulate the flow around the rod, the source is moved in order to simulate the here considered case which is equivalent to the flow around the source. Thus, the speed of the movement was set to the same flow velocity of the wind tunnel to make it comparable with the flow around the selected rod. Assuming that the acoustic radiation of a rod in a flow is a dipole and that the sound emission occurs at the same time along the rod length, the simulation was carried out in 2D and with a dipole as source. The amplitude, wave length and frequency of the source as well as the time resolution of the simulation were chosen exactly in accordance with the measured values used in the experiment (the detailed parameters are listed in the following chapters 3 and 4). The size of the computational domain was designed that the movement of the source could be resolved for several period lengths of the oscillating dipole and all observed PIV fields of view are completely covered. The movement of the source starts, after the initial acoustic propagation has reached the boundaries of the simulation domain. To simplify matters and as a first starting point, the source was treated as a point source neglecting the fact that the used rod had a defined diameter.

### 2.3 2D analytical solution of a dipole in uniform flow

For the analytical solution, the same assumptions are made, namely, that the source is a dipole which can be represented in a 2D domain. The convected wave equation serves as starting point for the calculation of the acoustic particle velocity $\boldsymbol{v}'$ in uniform flow. It is defined as follows

$$\frac{1}{c_0^2}\frac{D_0^2(\boldsymbol{\nabla}\cdot\boldsymbol{v}')}{Dt^2} - \Delta(\boldsymbol{\nabla}\cdot\boldsymbol{v}') = Q_v \tag{3}$$

with the material derivative $\frac{D_0}{Dt} := \frac{\partial}{\partial t} + \boldsymbol{v}_0\frac{\partial}{\partial \boldsymbol{x}}$, the speed of sound $c_0$, the Nabla-operator $\boldsymbol{\nabla}$ and the Laplace-operator $\Delta$. The term on the right-hand side can be regarded as the sources like point mass or heat and force sources, respectively. A reasonable way to solve this equation is to use one of the *Green's* functions. The required function for the 2D case in uniformly moving medium is given by

$$G_0^{2D}(\boldsymbol{x},t) = \frac{H\left(t-\tau+\frac{r}{c_0}\frac{M_r-\sqrt{1-\boldsymbol{M}^2+M_r^2}}{1-\boldsymbol{M}^2}\right)}{2\pi\sqrt{1-\boldsymbol{M}^2}\sqrt{\left[t-\tau+\frac{r}{c_0}\frac{M_r}{1-\boldsymbol{M}^2}\right]^2-\frac{r^2}{c_0^2}\frac{(1-\boldsymbol{M}^2+M_r^2)}{(1-\boldsymbol{M}^2)^2}}}. \tag{4}$$

Here the function $H$ denotes the Heaviside function, $t$ the time and $\tau$ the retarded time between the observer at position $\boldsymbol{x}$ and the source at point $\boldsymbol{\xi}$. Furthermore, $\boldsymbol{r} = \boldsymbol{x}-\boldsymbol{\xi}$, $M_r = \boldsymbol{M}\cdot\boldsymbol{r}/r$, $r = |\boldsymbol{r}|$ and $\boldsymbol{M}$ is the directional dependent Mach-number. Applying this Green's function on the convected wave equation, results in an analytical expression for the acoustic particle velocity of a mass or heat source in uniform flow for the 2D case (details of the derivation can be found in (9)):

$$\begin{aligned}\boldsymbol{v}'(\boldsymbol{x},t) = \frac{-\omega\theta_p}{4c_0\rho_0\sqrt{1-\boldsymbol{M}^2}^3}\Bigg\{&\left[\boldsymbol{M}J_0(kr^*)+\frac{(1-\boldsymbol{M}^2)\boldsymbol{e}_r+M_r\boldsymbol{M}}{\sqrt{1-\boldsymbol{M}^2+M_r^2}}Y_1(kr^*)\right]cos\left(\omega t+kr\frac{M_r}{1-\boldsymbol{M}^2}\right)\\&+\left[\boldsymbol{M}Y_0(kr^*)-\frac{(1-\boldsymbol{M}^2)\boldsymbol{e}_r+M_r\boldsymbol{M}}{\sqrt{1-\boldsymbol{M}^2+M_r^2}}J_1(kr^*)\right]sin\left(\omega t+kr\frac{M_r}{1-\boldsymbol{M}^2}\right)\Bigg\}.\end{aligned} \tag{5}$$

The functions $J_{0,1}$ are the *Bessel* functions of zeroth and first order while $Y_{0,1}$ stand for the *Neumann* functions of zeroth and first order. The additional variables are the angular frequency $\omega$, the wave number $k$, the reference density $\rho_0$ and $r^* = r\sqrt{1-\boldsymbol{M}^2+M_r^2}/(1-\boldsymbol{M}^2)$ while $\boldsymbol{e}_r = \boldsymbol{r}/r$. The quantity $\theta_p$ indicates the strength of the source.

This equation reflecting the analytical solution was implemented in a *MATLAB* script with specified parameters for the frequency, the Mach-number, the time resolution and the computational domain corresponding to the measurements of the experiment. Further details are listed in the following chapters. Since equation (5) describes the acoustic particle velocity propagation of a monopole, two sources were implemented in a distance equal to the rod diameter and with opposite

phase to realize a dipole.

## 3. EXPERIMENTAL SETUP

### 3.1 Flow configurations

The experiments were conducted in the Aeroacoustic Wind Tunnel Braunschweig (AWB) of the DLR, German Aerospace Center. The AWB is an open-jet closed-circuit anechoic test facility with a rectangular 0.8 by 1.2 m nozzle exit. Measurements have been performed at different rod configurations and a freestream velocity of $U_\infty = 60$ m/s. The Reynolds-number was $\mathrm{Re}_d \approx 60000$ based on the rod diameter of $d = 0.015$ m. A circular, semicircular and quadratic rod configuration as well as a combination of a circular and quadratic rod in a distance of 0.19 m behind one other were investigated. They were installed between end plates mounted on two opposing sides of the wind-tunnel nozzle. The span of all rods was $s = 0.8$ m. Every rod was additionally equipped with a pressure sensor (Type: 8507C-; Endevco) positioned at the half-span to measure the pressure fluctuations in the wake. To obtain optical access for PIV, one of the plates was made of borosilicate glass.

### 3.2 PIV measurements

The velocity data were acquired using a two-dimensional, two-component PIV system (2D2C-PIV) which measured two velocity components in different planes, orthogonal to the rod axis. The various regions of interest (ROI) were located at different positions in respect to the rod and the microphones, respectively, as illustrated in Figure 1.

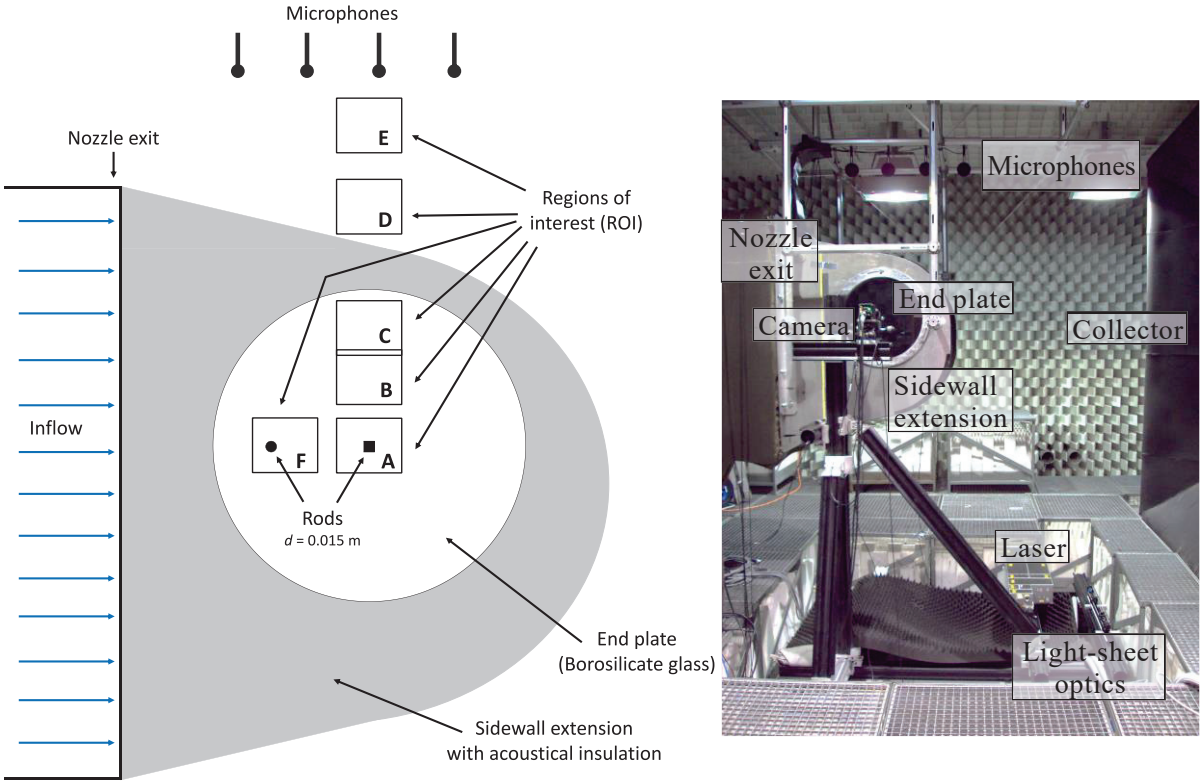


Figure 1 – Left: Schematic diagram of the side view of the experimental setup. The boxes A - F indicate the regions of interest (ROI) captured by the PIV camera. Right: Photograph of the experimental setup with designations.

The particle images were captured using a CMOS camera (PCO edge 5.5) with a resolution of 2560 px × 2160 px and a frame rate of 14 Hz in direct-to-disc storage mode. 15000 double frames were recorded for every configuration and ROI. DEHS particles were illuminated using a double-pulse laser (Q-switched Nd:YAG; Type: Innolas Spitlight 600) with a maximum energy of 350 mJ per pulse and a repetition rate of 14 Hz. The illumination of the ROI took place from diagonally below, downstream to the rods. The flow was seeded with diethylhexylsebacate (DEHS) tracer particles with

a mean particle diameter of approximately 1 µm. The seeding particles were injected from a corner of the wind tunnel upstream of the model configuration in a way that the particles had to pass the complete wind tunnel before they reached the ROI. The used camera lens and the geometry of the experimental arrangement resulted in a resolution of 23.1 px/mm. The PIV measurements were simultaneously conducted with the microphone recordings. Therefore, the signal of the camera was captured in order to subsequently assign the corresponding acoustic data to the respective frames. In the ROI A and F, the dynamic range of the PIV was approximately 46 dB to resolve the vortex structure in the wake of the rods. In the ROI B to E, much higher dynamic ranges were realized (e.g. in ROI C > 72 dB) to resolve the acoustic fluctuations in the flow emanating from the source region in the vicinity of the rods to the far field.

### 3.3 Far-field microphone measurements

The pressure measurements in the far field outside the flow were conducted with four microphones (Type: 1/2" 40AC; G.R.A.S.) arranged in a horizontal line above the rods. The vertical position was on a level with the half-span of the rods located at approximately 1 m (66.6 $d$) in y-direction. A multi-analyzer (Type: OR36; OROS) simultaneously recorded the microphone, the camera and the pressure sensor signals with a sampling frequency of $f_s = 51.2$ kHz and a dynamic range of 24 bit. All channels had an anti-aliasing filter at $f_u = 25.6$ kHz. To reduce the influence of low-frequency wind-tunnel noise on the measured signals, a high-pass filter with a cutoff frequency $f_l = 200$ Hz was used.

## 4. RESULTS AND DISCUSSION

In the following discussion, the flow direction is always from the left to the right. In case of the 2D simulation, the source moves from the right to the left. The axes are scaled with the rod diameter for better comparability in all contour plots. The case of the quadratic rod was chosen for the comparison since it delivered the highest absolute sound pressure level and, therefore, the radiated acoustic perturbations are most significant in this case. This means that only the PIV windows A to E are considered in the following discussion. The model contours are depicted in black and gray whereas the white areas indicate the masking of the PIV processing and the gaps between the fields of view. The data of the microphone directly above the rod was selected for calculating the cross-correlation function. Please note that mainly the velocity component $v$ pointing in the direction of the chosen microphone is considered. This is the main direction of the sound radiation produced by the flow around the rod.

### 4.1 Flow field

The velocity fluctuations gained by the PIV measurements are the basis for the calculation of the cross-correlation function. For this reason, the velocity data will be analyzed first, in order to obtain information on the general flow behavior. In figure 2, an instantaneous distribution of the velocity fluctuations $v'$ is depicted using a color code. The mean value $v_m$ has been subtracted. The flow field shows the *von Kármán* vortex street as expected for the wake of the rod (ROI A). Large-scale vortices with changing rotational direction are separating above and below the cylinder, emanating further downstream with a proximate distance of 1.8d to each other. The sign of the vertical velocity component $v'$ fluctuates in accordance with the periodically shed vortices. A detailed description of cylinder or rod wake flow fields and the involved characteristics including different rod geometries can be found in (2,10 – 12).

Considering the other regions of interest (ROI B - E), however, the velocity fluctuations are very low compared to the fluctuations in the wake flow. Only in the ROI D slightly higher variations in the $v'$ velocity component are visible due to the interaction of the wind

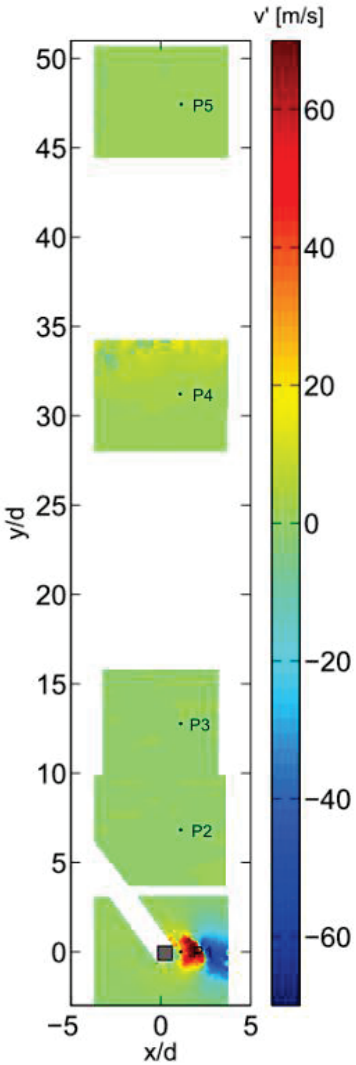


Figure 2 – Instantaneous velocity field of the $v'$ fluctuations.

tunnel flow with the resting ambient air, the so-called shear-layer. This observation is presented in figure 3 showing velocity fluctuations $v'$ of several consecutive PIV snapshots at different vertical positions on a virtual line at $x/d = 1$ (marked in figure 2).

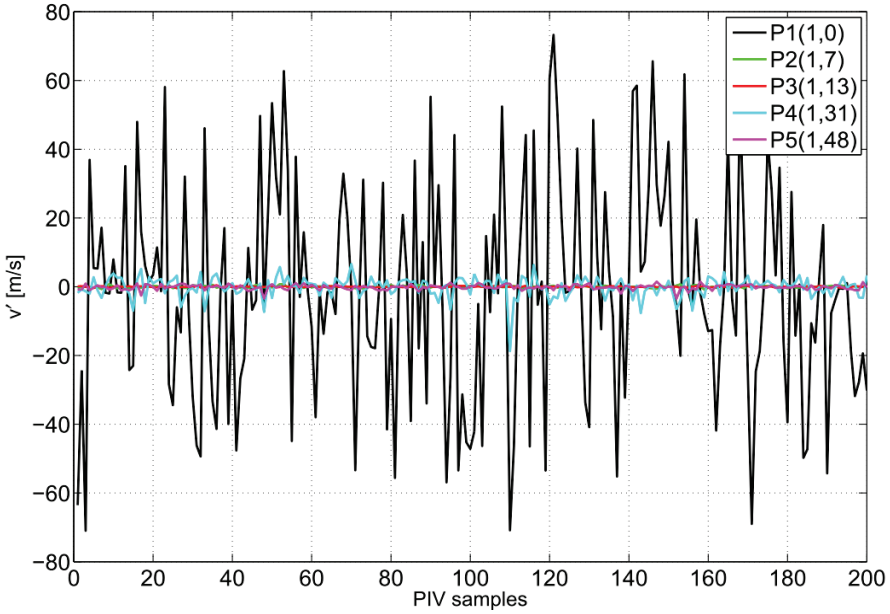


Figure 3 – Fluctuations of the v' component depending on the PIV sampling rate at different vertical positions in the flow field.

Therefore, it is evident that standard PIV measurements are not sufficient to resolve the acoustic perturbations. This could be probably solved using the recently presented progress on time resolved particle tracking velocimetry (PTV) (cf. (13)). Hence, the simultaneous measurement of the velocity in the flow and the acoustic fluctuations in the far field is applied in this study. The velocity fluctuations are quasi seeded with the acoustic information and only flow variations are significantly correlating with the far-field pressure signal.

### 4.2 Acoustic results

In order to calculate the acoustic frequency spectrum, a section of ~470 s of the microphone signal has been cut into 1200 equal parts with 50% overlap. A *Hanning* window was applied on every signal part before computing the *Fourier* transformation. The corresponding frequency resolution is ~1.3 Hz.

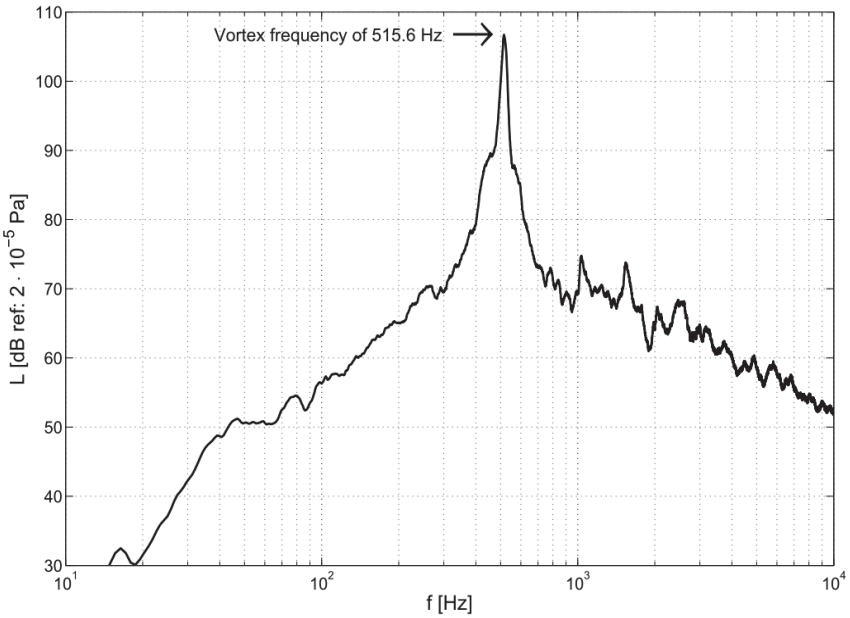


Figure 4 – Sound pressure level of the flow around a quadratic rod measured in the far field using a microphone.

The average of all parts is used for the sound pressure level calculation which is given in decibels with a reference pressure of $p_{ref} = 2 \cdot 10^{-5}$ Pa. The resulting spectrum is shown in figure 4 in which the frequency axis is scaled logarithmically.

The tonal component of the vortex frequency is dominant at approximately 515 Hz produced by the *von Kármán* vortex street. This is also the frequency used for the numerical simulation and analytical solution, respectively. Furthermore, additional harmonics are reflected, though with a much lower sound pressure level. The distinct tonal component of the acoustic response reflects a strong and clear propagation of the acoustic particle velocity which should be identified with the used measurement technique. The application of the cross-correlation between the velocity and the acoustic data serves as proxy variable to achieve this goal. The calculation scheme as well as the corresponding result are presented in the following section.

### 4.3 Cross-correlation results

Using the procedure sketched in figure 5, the cross-correlation function (cf. equation (1) of section 2.1) was calculated. Time windows of $-40\,\text{ms} \leq \tau \leq 40\,\text{ms}$ of the pressure signal around the time $t_i$ of the separate PIV snapshots were extracted from the complete signal and multiplied by the associated velocity data of the PIV measurements. The output signal of the camera was chosen as the reference time $t_i$. Please note that the velocity fields were measured with a sufficiently low sampling rate (14 Hz – cf. section 3.2.) to ensure that the consecutive PIV recordings are statistically independent (cf. (2)). Only this guarantees that the information gain is maximized for the time-averaged statistical quantity with every PIV sample.

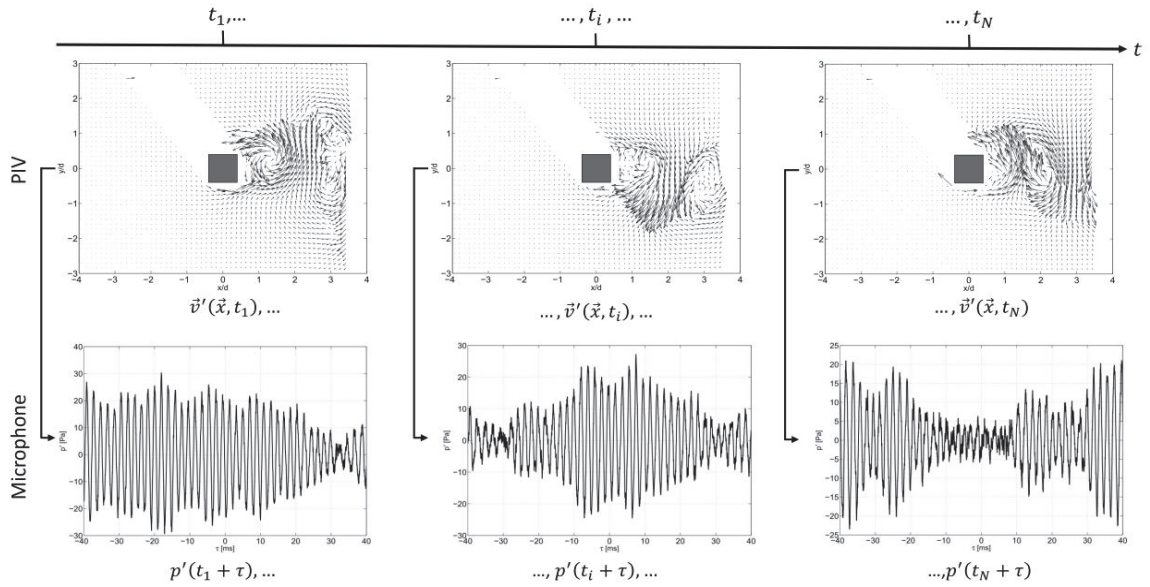


Figure 5 – Scheme of the cross-correlation calculation between the recorded velocity fluctuation in the flow with the PIV technique and the pressure fluctuations in the far field using a microphone.

As a last step, the results of the multiplications are summed up and divided by the total amount of PIV samples. Thus, the resulting cross-correlation function obtains the time resolution from the sampling rate of the microphone measurement and the spatial resolution from the PIV recording.

In figure 6, several results of the described procedure are presented. Instantaneous distributions of the scaled cross-correlation function (cf. equation (2) of section 2.1) are depicted using a color code for different points in time $\tau$. At first glance, the large-scaled coherent structures with alternating sign symmetry along $y = 0$ are remarkable. They develop in the direct vicinity of the rod and are convected downstream with a well-defined group velocity (cf. (2)). This observation is causally linked to the vortex convection of the emanating *von Kármán* vortices. The observed topology of the correlation values can be explained by the strong spatial coherence of the flow structures in the rod wake. The coherent structures are part of the same physical process causing the pressure oscillations in the far field. The described structures reflect the periodicity of the *von Kármán* vortex street containing the detected vortex frequency.

It is interesting to note that in the area upstream the rod ($x/d < 0$) high correlation values can be observed with a much higher propagation velocity than downstream. It is assumed here that mainly harmonic oscillations are causing velocity fluctuations. These fluctuations are not superimposed by turbulent motions in the flow and exhibit a strong coherence with the fluctuations downstream of the rod (cf. (2))

The differences of the distributions of the cross-correlation function (proxy variable for the acoustic particle velocity) presented for three time instances in figure 6 reflects the wave propagation. Solely in the shear-layer ( $31 \leq y/d \leq 35$) is the traceability disturbed due to the random particle motions not related to the acoustic propagation. Furthermore, the decay behavior of the acoustic perturbations becomes visible with increasing distance to the source region. In the following section, the results obtained with the cross-correlation function approach are compared with those of the 2D simulation and the 2D analytical solution of a dipole with regard to the acoustic particle velocity to validate the proposed approach.

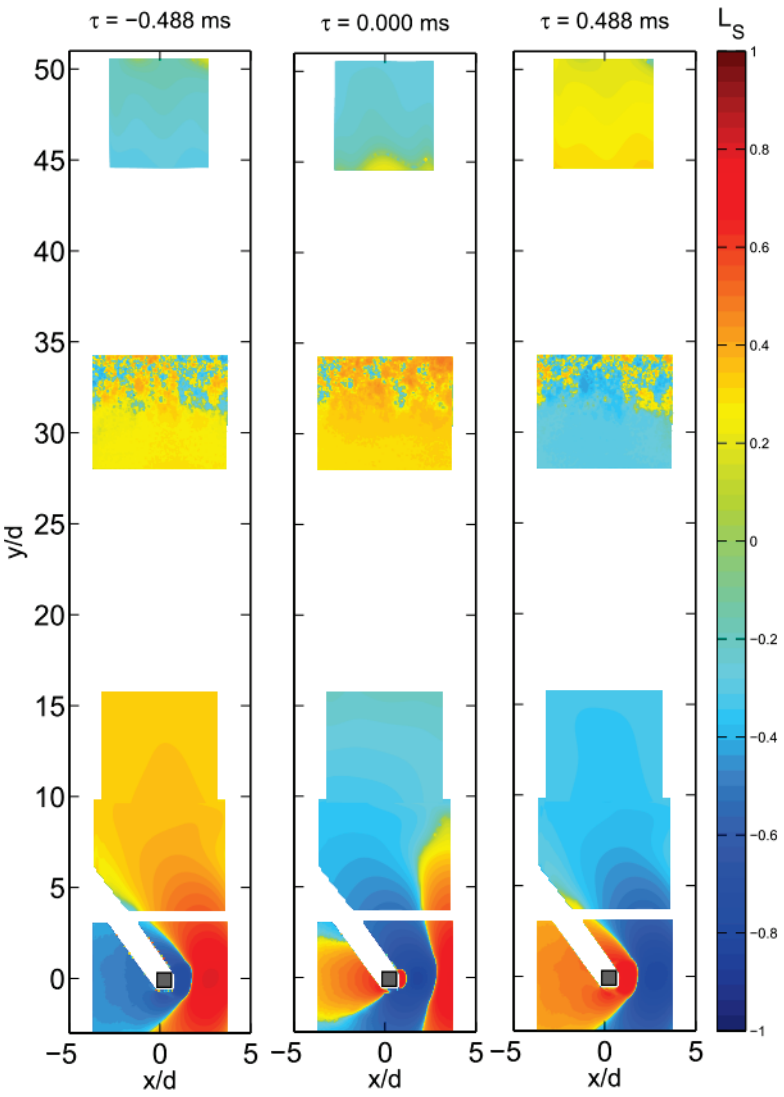


Figure 6 – Instantaneous distributions of the cross-correlation function for different points in time $\tau$.

### 4.4 Comparison of the results of the measurement, the numerical simulation and the analytical solution

In the following, the acoustic particle velocity obtained in the numerical simulation and from the analytical solution is scaled in accordance to the cross-correlation function. Only the scaling factor differs due to the disparate magnitude of the considered variable. It is defined as follows:

$$L_v = \underbrace{sgn(v') \cdot log\left(\frac{|v'|}{v_0}\right)}_{L_v^*} / max(|L_v^*|). \tag{6}$$

where $v'$ is the calculated acoustic particle velocity and $v_0 = 5 \cdot 10^{-8}\,\mathrm{m/s}$ the reference particle velocity in air. The application of the absolute value on $v'$ is also necessary due to the oscillation between positive and negative values. Therefore, the direction of the velocity is maintained in the sign function. The normalization with the global maximum value ensures a uniform scale between 1 and -1 in order to be able to compare them to the presented results of the cross-correlation function.

In figure 7 the color-coded instantaneous distributions of the scaled acoustic particle velocity obtained in the numerical simulation and the analytical solution considering a dipole are presented. The used frequency of the dipole is the measured vortex frequency and the amplitude is based on the measured sound pressure level. Furthermore, the time resolution is adapted to the sampling rate of the

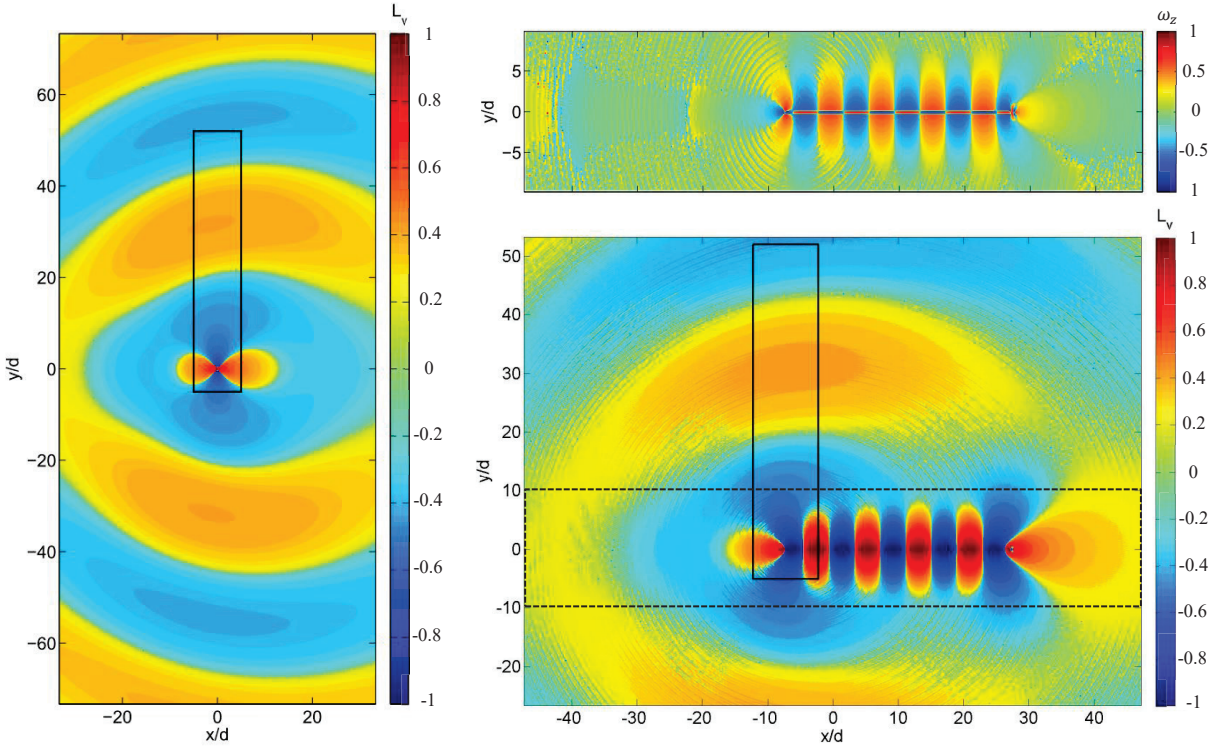


Figure 7 – Instantaneous distributions of the acoustic particle velocity obtained by the computation of the 2D analytical solution (left) and the 2D simulation (right bottom) of a dipole, respectively. The solid line rectangles indicate the regions investigated by the PIV system. The dashed line rectangle represents the area for which the vorticity is calculated (right top).

microphone measurements ($dt = 1/f_s$) and the Mach-number is in accordance with the wind tunnel velocity ($M = U_\infty/c_0$). In the case of the analytical solution, an asymmetry can be observed along $x/d = 0$ due to the predominant uniform flow. Convected flow structures emanating from the source region upstream are not existent because the analytical solution is a pure acoustic model without vortex presence and interaction. However, the velocity propagation is reflected which makes it useful as a case for comparison.

Considering the results of the numerical simulation, one observes that the intensity of the vortices in the wake of the dipole does not decay. The vortices are obviously produced by the movement of the source. Though, by solving the *Euler* equations instead of the *Navier-Stokes* equation, molecular dissipation which is responsible for their decay is not modelled. This can be seen in the diagram right top of figure 7 in which the calculated vorticity ($\omega_z = \partial v'/\partial x - \partial u'/\partial y$) is depicted. The strength of the vorticity does not decay with increasing distance to the source which is an indicator for the missing dissipation. Nevertheless, the behavior of the acoustic particle velocity production and propagation is similar to those obtained by the cross-correlation function values.

The rectangular areas indicated by the black frames are the areas which includes all PIV fields of view. The data in these areas are used for the comparison with the results of the cross-correlation approach. Snapshots of the acoustic particle velocity distributions obtained by the analytical solution and by numerical simulation are compared with the cross-correlation function in. figure 8 using color-coded contours. The comparison reveals that the cross-correlation function reflects the wave propagation in a similar manner as the acoustic particle velocity. Since the analytical solution does not contain the generation of vortices, the difference to the experimental and numerical results are large close to the rod where the *von Kármán* vortices are generated.

In order to highlight that the results obtained by the different approaches are similar, a temporal evolution of the values along a vertical line at $x/d = 1$ (indicated by the dashed lines in Figure 8) is depicted in figure 9. The $y$-axis shows the vertical position while the $x$-axis denotes the time. It can be observed that all three approaches reflect the same periodicity as expected. Inclined lines emanate above the turbulent region near the source $(y/d > 10)$ containing the information about the speed of sound. Only the lines showing the values obtained with the cross- correlation approach reflect disturbances caused by the shear layer. In the region around the source $(-5 \leq y/d \leq 5)$, the general behavior is similar although there are distinct differences in detail. Also remarkable is the transition area around $5 \leq y/d \leq 10$ in which the propagation velocity is higher than the speed of sound in the cases of the cross-correlation values and the analytical solution. Based on this comparison, it can be concluded that the used measurement technique and the chosen approach apparently are suitable to resolve the acoustic wave propagation of a strong tonal noise source from the near to the far field with present flow.

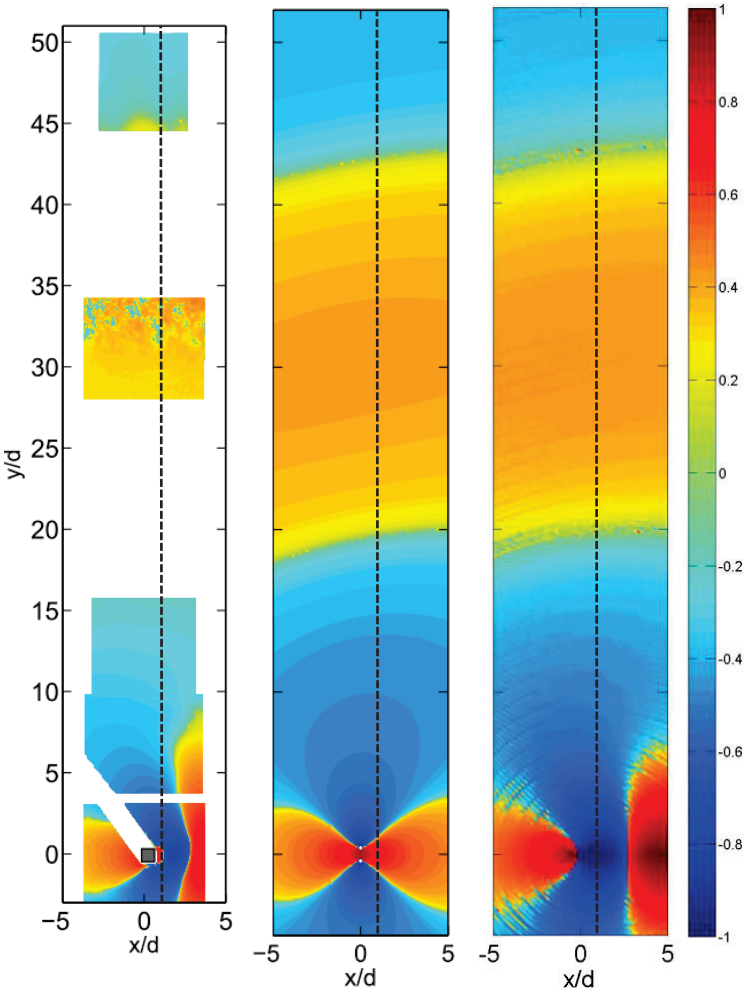


Figure 8 – Snapshot of instantaneous distributions of the cross-correlation function (left), the analytical solution (middle) and the numerical simulation (right). The dashed lines indicate positions for further evaluations.

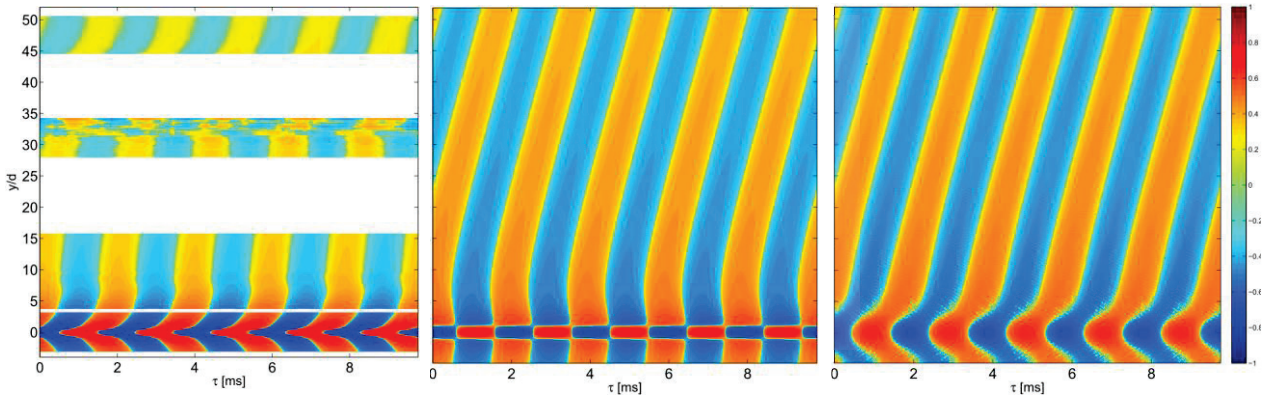


Figure 9 – Temporal evolution of the cross-correlation function (left), the analytical solution (middle) and the simulation (right) along the vertical line at $x/d = 1$.

## 5. CONCLUSIONS

The generation and propagation of the acoustic particle velocity have been successfully investigated by means of synchronized velocity measurements in the flow field using the PIV technique and pressure recordings in the far field via microphones. The cross-correlation function between these two quantities served as a proxy variable for the acoustic particle velocity. The acoustic wave propagation of a strong tonal noise source produced by a uniform flow around a quadratic rod could be resolved and reproduced from the near field in the vicinity of the source through the shear layer of the wind tunnel flow to the acoustic far field. The validity of the used approach were examined by the comparison with a 2D simulation as well as a 2D analytical solution of an appropriate dipole. The propagation behavior of all three cases is in good agreement.

## REFERENCES

1. Siegel L, Ehrenfried K, Henning A, Wagner C. Intensity-Analysis of Cross-Correlated Synchronized PIV and Microphone Measurements. 11th Int Symp on Particle Image Velocimetry. Santa Barbara, CA USA; 2015.
2. Henning A, Koop L, Ehrenfried K. Simultaneous Particle Image Velocimetry and Microphone Array Measurements on a Rod-Airfoil Configuration. AIAA J. 2010;48(10):2263–73.
3. Henning A, Kaepernick K, Ehrenfried K, Koop L, Dillmann A. Investigation of aeroacoustic noise generation by simultaneous particle image velocimetry and microphone measurements. Exp Fluids. 2008;45:1073–85.
4. Schröder A, Herr M, Lauke T, Dierksheide U. Measurements of Trailing-Edge-Noise Sources by means of Time-Resolved PIV. 6th International Symposium on Particle Image Velocimetry. Pasadena, California, USA; 2005.
5. Koschatzky V, Moore PD, Westerweel J, Scarano F, Boersma BJ. High speed PIV applied to aerodynamic noise investigation. Exp Fluids. 2011;50:863–76.
6. Treeby BE, Jaros J, Rendell AP, Cox BT. Modeling nonlinear ultrasound propagation in heterogeneous media with power law absorption using a k -space pseudospectral method. J Acoust Soc Am. 2012;131(6):4324–36.
7. Treeby BE, Cox BT. Modeling power law absorption and dispersion for acoustic propagation using the fractional Laplacian. J Acoust Soc Am. 2010;127(5):2741–8.
8. Treeby BE, Cox BT. k-Wave : MATLAB toolbox for the simulation and reconstruction of photoacoustic wave fields. J Biomed Opt. 2010;15(2):021314.
9. Delfs J. Basics of Aeroacoustics (Lecture notes) Technische Universität Braunschweig; 2014. 134 p. /
10. Williamson CHK. Vortex Dynamics in the Cylinder Wake. Annu Rev Fluid Mech. 1996;28:477–539.
11. Zdravkovich MM. Flow around Circular Cylinders, Part I. 1. Edition. Oxford science publications; 1997.
12. Iglesias EL, Thompson DJ, Smith MG. Experimental study of the aerodynamic noise radiated by cylinders with different cross-sections and yaw angles. J Sound Vib
13. Schanz D, Gesemann S, Schröder A. Shake-The-Box : Lagrangian particle tracking at high particle image densities. Exp Fluids. Springer Berlin Heidelberg; 2016;57(70).